

Chemical Science

Accepted Manuscript



This is an *Accepted Manuscript*, which has been through the Royal Society of Chemistry peer review process and has been accepted for publication.

Accepted Manuscripts are published online shortly after acceptance, before technical editing, formatting and proof reading. Using this free service, authors can make their results available to the community, in citable form, before we publish the edited article. We will replace this *Accepted Manuscript* with the edited and formatted *Advance Article* as soon as it is available.

You can find more information about *Accepted Manuscripts* in the [Information for Authors](#).

Please note that technical editing may introduce minor changes to the text and/or graphics, which may alter content. The journal's standard [Terms & Conditions](#) and the [Ethical guidelines](#) still apply. In no event shall the Royal Society of Chemistry be held responsible for any errors or omissions in this *Accepted Manuscript* or any consequences arising from the use of any information it contains.

Cite this: DOI: 10.1039/c0xx00000x

www.rsc.org/xxxxxx

ARTICLE TYPE

Investigation on Photo-Induced Charge Separation in CdS/CdTe Nanopencils

Masanori Sakamoto,^{*a,b} Koki Inoue,^c Masaki Saruyama,^c Yeong-Gi So,^d Koji Kimoto,^c Makoto Okano,^a Yoshihiko Kanemitsu,^a Toshiharu Teranishi^{*a}⁵ Received (in XXX, XXX) Xth XXXXXXXXXX 20XX, Accepted Xth XXXXXXXXXX 20XX

DOI: 10.1039/b000000x

CdS/CdTe nanopencils were synthesized via anion exchange. The effect of geometry on carrier dynamics was investigated. Transient absorption measurements indicated these factors did not affect the charge separation rate in CdS/CdTe nanopencils. The results provide important insight for designing heterostructured nanocrystals with efficient charge separation and integrated structures.

Introduction

Geometric structure has a strong bearing on the properties of semiconductor nanocrystals (NCs). This is because NC band structure and carrier dynamics are affected by their size and shape. Synthesizing NCs composed of two or more chemical species significantly expands available NC geometric structures and functionality. Composite NCs include alloy, core/shell (isotropic phase segregation), and hetero (anisotropic phase segregation) structures. Fusing and/or integrating multiple functionality NCs can impart unique and synergetic properties.¹⁻⁴ Heterostructured NCs (HNCs) are promising materials in photoelectric conversion systems, sensors, and catalysts. This is because of the combined effect of independent functional units, and/or efficient carrier transfer between phases.⁴⁻⁶ The anisotropic structure of HNCs favors directed carrier transfer and the construction of ordered suprastructures.⁵⁻⁹ Moreover, the anisotropic phase segregation is favourable for the long carrier lifetimes, which is attributed to the spatial separation of the electron and hole between the distinguished phases. Klimov et al. reported that PbSe/CdSe/CdS heteronanotetrapods showed the long-lived charge separation compared with the PbSe/CdSe core shell NCs.⁵ Han et al. reported that the Cu_{1.94}S/CdS and Cu_{1.94}S/ZnxCd_{1-x}S heteronanodisk shows the efficient charge separation.⁹ Quantum confinement exhibited by the segregated phases enables the band alignment in HNCs to be controlled. Understanding the relationship between geometry (shape, volume, and heterointerface area) and carrier dynamics in HNCs is important for controlling photo-generated carriers in HNCs for practical use. Synthesizing HNCs with precisely controlled sizes and shapes remains a significant challenge to achieving this.

Herein, we report phase-segregated CdS/CdTe heterostructured nanopencils (HNPs), with controlled anisotropic structure and CdS/CdTe volume. We investigated the relationship between their geometry and photo-induced carrier dynamics. The

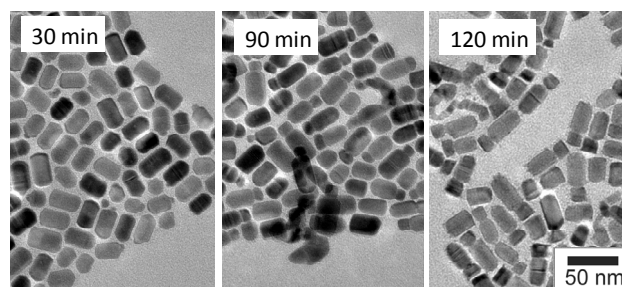
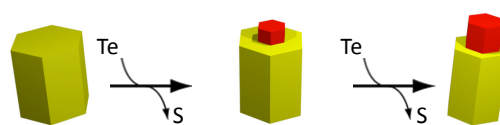


Fig. 1 TEM images of CdS/CdTe HNCs obtained by the anion exchange of CdS nanopencils with TOP=Te, at 260 °C for 30–120 min.

CdS/CdTe HNCs possess type-II band alignment, in which CdTe serves as a light-absorbing layer. The HNCs were formed through the anion exchange of CdS nanopencils. CdS nanopencils are wurtzite hexagonal prisms, grown along the [001] direction. They are a promising building block, because their six-fold symmetry can form extended honeycomb structures.¹⁰ The HNP crystal structure and formation mechanism were investigated by transmission electron microscopy (TEM), high-angle annular dark-field (HAADF) scanning transmission electron microscopy (STEM), and X-ray diffraction (XRD). We also investigated how geometry influences photo-induced charge separation in CdS/CdTe HNCs. The volume of CdTe and shape of CdS/CdTe HNPs were changed, and compared with smaller spherical CdS/CdTe heterodimers. This was achieved by transient absorption measurements, using femtosecond (fs)-laser flash photolysis.

Seeded growth and ion exchange reactions have been developed to synthesize HNCs.¹¹⁻¹³ Ion exchange is a simple and convenient strategy for synthesizing HNCs with precise geometries.¹³⁻¹⁵ We first synthesized CdS nanopencils for use as HNP seeds. We previously synthesized CdS nanopencils through the thermal Ostwald ripening of zinc blend (zb) spherical CdS, in the presence of Cl⁻.¹⁰ Herein, this two-step method was modified into a one-step reaction (S.I.). The nanopencils are 17 ± 2 nm wide and 30 ± 4 nm long (Fig. S1). Their XRD pattern is

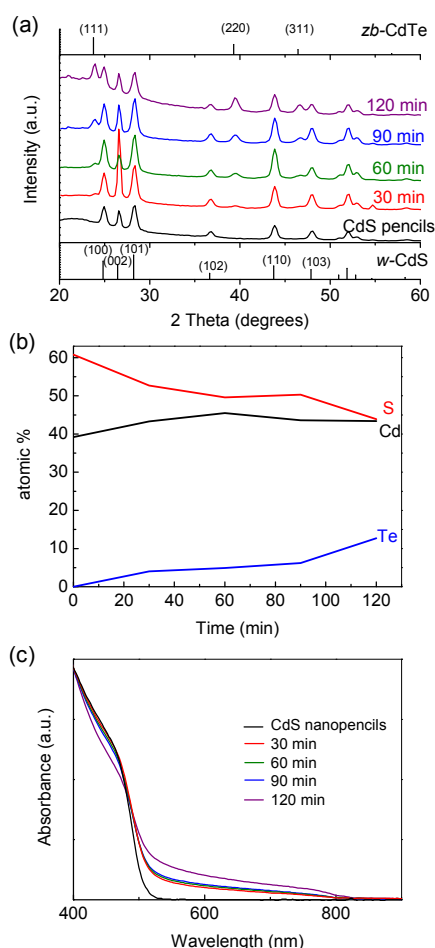


Fig. 2 Time evolution changes in (a) powder XRD patterns (b) compositions estimated by XRF, and (c) absorption spectra of nanopencils during anion exchange.

characteristic of a wurtzite (*w*) structure (Fig. S2). Their optical absorption edge indicates a band gap energy of 2.5 eV, typical of bulk CdS (Fig. S3).

The anion exchange of CdS NCs with alkylphosphine chalcogenides ($R_3P=E$, E:Se, Te) is a powerful strategy for synthesizing HNCs.¹² The binding energy between P and the chalcogen decreases in the order $S > Se > Te$. The thermal energy over the potential energy barrier for bond cleavage leads to the exchange of S in CdS with Se or Te. We used anion exchange in CdS nanopencils to form CdS/CdTe HNCs, where CdS nanopencils were heated at 260°C in the presence of trioctylphosphine telluride (TOP=Te). The anion exchange of CdS with TOP=Te in oleylamine formed heterostructures, whilst maintaining the nanopencil shape (Fig. 1). As the reaction proceeded, the new phase formed and grew within the width of the seed nanopencil. CdTe only grew on one side of the CdS nanopencils. The hexagonal prism shape of the seed nanopencils was preserved during exchange. The CdS/CdTe volume ratio could be tuned by the reaction time, because anion exchange took longer than cation exchange, because of the larger anion radius.

We then characterized the CdS and CdTe phases and CdS/CdTe heterointerface in the HNCs. The time evolution XRD patterns of the products are shown in Fig. 2a. Diffraction peaks characteristic of *zb*-CdTe (111), (220), (311) emerge with

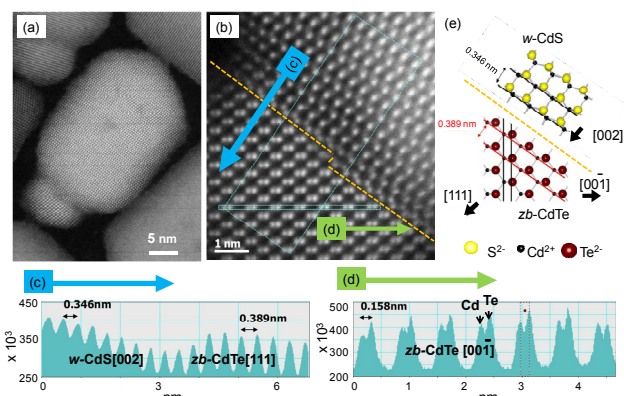


Fig. 3 Atomic-resolution HAADF-STEM images of (a) a CdS/CdTe HNP and (b) the CdS/CdTe heterointerface. Z-contrast profiles of anion/cation columns in the light blue rectangular regions marked (c) by the blue arrowhead and (d) by the green arrowhead, in Fig. 3(b). (e) Schematic of the *w*-CdS/*zb*-CdTe heterointerface.

increasing reaction time. This indicates that the CdTe phase was formed through anion exchange, without any solid solution phases. Evolution of the products was also monitored by X-ray fluorescence (XRF) analysis (Fig. 2b). The mole fractions of S and Te monotonically decrease and increase with increasing time, respectively. This indicates that S^{2-} is gradually exchanged by Te^{2-} . An absorption shift with increasing time indicates that exchange results in the decrease of CdS absorption, and the emergence of an absorption band edge at ~ 860 nm, which is characteristic for CdTe (bulk band gap 1.44 eV) (Fig. 2c).

HAADF-STEM images of CdS/CdTe HNCs obtained after 30 min reaction (Fig. 3a–d and S4) show two anisotropically segregated phases with different lattice spacings. The brightness of HAADF-STEM images is proportional to the square of the mean atomic number (*Z* contrast). Bright and dark spots observed in the HNCs correspond to Te ($Z = 52$) and Cd ($Z = 48$) in CdTe, and Cd ($Z = 48$) and S ($Z = 16$) in CdS, respectively (Fig. 3b–d). From the atomic stacking, large and small phases in the HNCs are assigned as *w*-CdS and *zb*-CdTe, respectively. The lattice spacing indicates that the lattice directions of *w*-CdS and *zb*-CdTe to the heterointerface are [002] and $[\bar{1}\bar{1}\bar{1}]$, respectively (Fig. 3c). Cd^{2+}/Te^{2-} columns can be discriminated from the *Z* contrast profile (Fig. 3d). The contact between the phases can be determined by the alignment of atoms near the heterointerface. (001) Facets of *w*-CdS contact with $(\bar{1}\bar{1}\bar{1})$ facets of *zb*-CdTe to form the interface (Fig. 3e).

The formation of a solid solution versus a heterostructured crystal was determined by the mutual solubility limits of the two phases as well as interfacial energies. The driving force for the formation of the anisotropically phase-segregated structure is believed to be the large lattice mismatch between *w*-CdS and *zb*-CdTe (11%). In CdE (E = S, Se, Te), a Cd and E pair can be defined as one crystal layer (a single bilayer). Zinc blende and wurtzite sequences are typically expressed as ABCABC and ABABAB, respectively (where each letter represents a bilayer). The deposition of *zb*-CdTe onto planes parallel to the *c* axis of *w*-CdS ($\{100\}$ and $\{110\}$) is strongly inhibited, because the atomic positions do not conform symmetrically. Consequently, the *zb*-CdTe phase preferentially connects to *w*-CdS $\{002\}$ facets, which are crystallographically equivalent to $\{111\}$ facets of the *zb*-

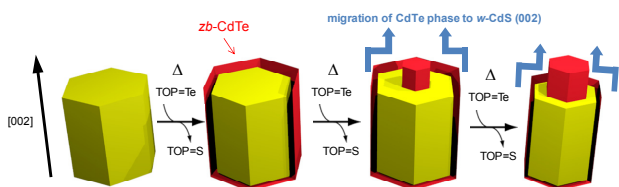


Fig. 4 Schematic illustration of the CdS/CdTe HNP formation mechanism.

lattice (threefold-symmetric configuration of cations and anions).

The CdS/CdTe HNPs have only one heterointerface, because of the lack of inversion symmetry along the c axis of w -CdS. The (001) and (00 $\bar{1}$) end facets of w -CdS are crystallographically nonequivalent, because the (001) and (00 $\bar{1}$) planes are terminated by Cd $^{2+}$ and S $^{2-}$, respectively. Te $^{2-}$ is a softer base than S $^{2-}$, and its ionic radius is larger than that of S $^{2-}$. Thus, Cd $^{2+}$ tends to form the interface with Te $^{2-}$ from (1 $\bar{1}\bar{1}$) end facets of zb -CdTe, rather than with S $^{2-}$ from (00 $\bar{1}$) end facets of w -CdS. In addition, the exposure of (111) end facets of zb -CdTe is preferable for electron donating oleylamine or TOP, as Cd $^{2+}$ from (111) end facets rather than Te $^{2-}$ from (1 $\bar{1}\bar{1}$) end facets. This suggests that the boundary formation between the end facets of w -CdS (001) and zb -CdTe (1 $\bar{1}\bar{1}$) is energetically favorable, compared with that formed between w -CdS (00 $\bar{1}$) and zb -CdTe(111).

The formation mechanism of the CdS/CdTe HNPs was investigated by monitoring their growth. Possible formation processes are i) preferential anion exchange from (001) facets of w -CdS, and ii) (001) facet selective migration of CdTe, generated by anion exchange on the whole w -CdS surface regardless of facets (Fig. 4). The latter is considered more likely. First, monitoring the initial CdS/CdTe HNPs formation shows that the CdTe/CdS interface area is smaller than that of the (001) facets of CdS. This infers that CdTe does not epitaxially grow from whole (001) facets of CdS. Second, the exposure of Cd $^{2+}$ on (001) facets of CdS is unfavorable for surface anion exchange. This is because protecting oleylamine or TOP groups strongly attach to Cd $^{2+}$, inhibiting access by TOP=Te. These observations support the stepwise formation mechanism of the anisotropically segregated structure, through the anion exchange and migration of CdTe. Our previous study found that CdS/CdTe heterodimers were formed from w -CdS nanospheres through a similar mechanism.¹²

Transient absorption (TA) measurements of the HNPs were carried out to investigate the structure-dependent photo-induced carrier dynamics, upon the excitation of CdTe. We examined factors affecting charge separation. These included the CdTe band gap energy, which was tuned by the size, and the geometry including volume, heterointerface area, and shape. Three representative HNPs with different CdS/CdTe volume ratios and geometries (#1, #2 and #3) were selected to investigate the relationship between geometry and the rate of charge separation (k_{el}) (Table 1 and S.I.). The CdS phases of all three samples are larger than twice the CdS Bohr radius (3 nm), and exhibit no quantum confinement (see CdS nanopencil absorption spectrum, S.I.). In contrast, the size of CdTe in #1 and #2 are smaller than twice the Bohr radius (6.8 nm). The CdTe band gaps estimated from Tauc's extrapolation of plots of $(ah\nu)^2$ against $h\nu$ are 1.6, 1.6, and 1.5 eV for samples #1, #2, and #3, respectively (S.I.).

This indicates that quantum confinement increases the CdTe

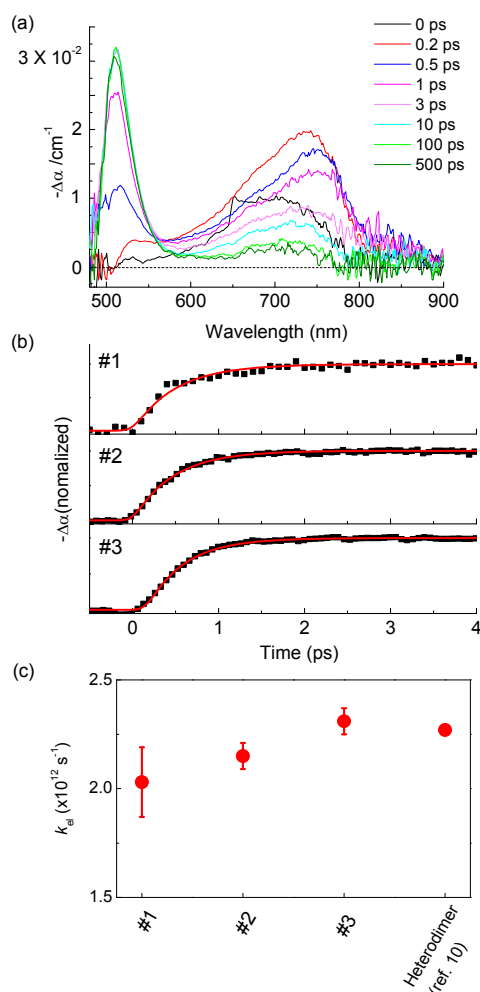


Fig. 5 (a) Representative time-resolved TA spectra of CdS/CdTe HNPs ($\lambda_{\text{pump}} = 651$ nm). The absorption spectrum at 0 ps is caused by the pulse width of laser (0.2 ps). (b) Kinetic traces of CdS state-filling signals (510 nm), after photoexcitation of CdTe in samples #1, #2, and #3. (c) k_{el} of samples #1, #2, and #3 and the heterodimer.

band gap in samples #1 and #2. The CdTe/CdS volume ratios are estimated to be 0.02, 0.1, and 0.4 for samples #1, #2, and #3, respectively. The HNP heterointerface areas are 25, 72, and 256 nm 2 for samples #1, #2, and #3, respectively.

Fig. 5a shows typical time-resolved TA spectra of CdS/CdTe HNPs (sample #2), during the selective excitation of CdTe at 651 nm. To suppress many particle effects such as Auger recombination, relatively low excitation intensities were used, which correspond to a linear power dependence (6.4–155 $\mu\text{J m}^{-2}$ per pulse). Upon excitation (0 ps), bleaching of the CdTe band corresponding to the 1S $_{3/2}(\text{h})$ –1S(e) and 2S $_{3/2}(\text{h})$ –1S(e) exciton states is observed.^{16,17} At 0.5 ps, the conduction band electron and valence band hole fall to the 1S(e) and 1S $_{3/2}(\text{h})$ energy levels, respectively. This gives rise to the dominant bleaching at the 1S $_{3/2}(\text{h})$ –1S(e) transition, which is expressed by the red-shift in the bleaching spectrum. At the same time, significant transient bleaching at ~ 510 nm is attributed to the state filling of the lowest energy 1S(h)–1S(e) transition in CdS. This spectral shift is associated with the CdS and CdTe exciton transitions by excitation-induced state filling, i.e., charge separation from

Table 1. CdS:CdTe volume ratios and k_{el}

Name	CdTe/CdS volume ratio	Interface area (nm ²)	k_{el} (10 ¹² s ⁻¹)
#1	0.02	25	2.03 ± 0.16
#2	0.10	72	2.15 ± 0.06
#3	0.37	256	2.31 ± 0.06

TEM images and detailed geometrical parameters of samples #1- #3 were shown in S.I.

excited CdTe to CdS. The conduction band of bulk CdS is approximately 0.35 eV lower than that of bulk CdTe.¹⁸ Type II band alignment is favorable for transporting electrons in the CdTe conduction band to CdS. The large CdS phase allows electron localization, and promotes the efficient photo-induced electron-hole separation. After 0.5 ps, bleaching signals linearly decay, which lasts much longer than the time window afforded by the present instrument. Above spectral shift largely reflects electron hole recombination between CdS and CdTe.

The influence of geometry on the charge separation behavior was investigated by TA kinetic traces obtained at the lowest energy bleaching position of CdS (510 nm) for samples #1, #2, and #3 (Fig. 5b). Time-evolution traces of CdS bleaching extract the component of charge separation, from the multiple decay processes of excited CdTe. From the TA kinetic trace, k_{el} is estimated to be $(2.03 \pm 0.16) \times 10^{12}$, $(2.15 \pm 0.06) \times 10^{12}$, and $(2.31 \pm 0.06) \times 10^{12}$ s⁻¹ for samples #1, #2, and #3, respectively (Fig. 5c). The slight increase in k_{el} with increasing CdTe fraction could potentially be within the error range. This indicates that neither quantum confinement nor geometry differences in the samples affect k_{el} . The k_{el} values of CdS/CdTe HNPs are similar to that of CdS/CdTe heterodimers (2.27×10^{12} s⁻¹).¹² The crystal structure and heterointerface of the HNPs are similar to those of the CdS/CdTe heterodimers, so these factors are likely to be more important than geometry in determining k_{el} .

The reasons for this insensitivity to geometry are now discussed. We exclude the contribution of electron diffusion in CdTe to k_{el} . Because diffusion is sufficiently fast it can be ignored on the charge separation time scale. This also explains why interfacial area does not affect k_{el} . k_{el} is faster than typical solvent reorganization rates, so charge separation proceeds via electron tunneling or strongly adiabatic electron transfer. Interfacial potential energy barriers of HNCs are caused by lattice strain, and can generally be thermally overcome at RT.^{19,20} This infers that tunneling could be eliminated at RT. We suggest that charge separation proceeds in a strongly adiabatic electron transfer. k_{el} is largely determined by the CdS density of states, and is largely independent of the total free energy change (ΔG) during charge separation.^{16,21} The density of states of the CdS phases are similar, so k_{el} in the three samples are also similar. We only investigated a very small range of quantum confinement in CdTe, here. The larger degrees of quantum confinement may cause significant change of electrontransfer efficiency. Further investigation including the temperature dependence is underway, to reveal the charge separation mechanism.

Conclusions

In summary, shape and size are not critical factors determining the charge separation rate in the present CdTe/CdS HNCs. This is because of the fast electron diffusion in CdTe, and ΔG -insensitive

charge separation. The heterointerface is more important than shape or CdTe/CdS volume ratio in determining k_{el} . This fact provide us an important insight designing HNCs exhibiting efficient charge separation, and have a useful structure for nano-building block.

ACKNOWLEDGMENT

We thanks to S. Taguchi for the fruitful discussions. This study was supported by a KAKENHI Grant-in-Aid for Scientific Research A (No. 23245028) (T.T.) (No.25240752) (Y.K.), a Grant-in-Aid for Scientific Research C (No. 25390017) (M.S.), JST-CREST (Y.K.) and The Sumitomo Electric Industries Group CSR Foundation (Y.K. and M.O.).

Notes and references

- ^aInstitute for Chemical Research, Kyoto University, Gokasho, Uji, Kyoto 611-0011, Japan. E-mail: sakamoto@scl.kyoto-u.ac.jp, teranishi@scl.kyoto-u.ac.jp
- ^bPRESTO, Japan Science and Technology Agency (JST), 4-1-8 Honcho Kawaguchi, Saitama 332-0012, Japan.
- ^cGraduate School of Pure and Applied Sciences, University of Tsukuba, 1-1-1 Tennodai, Tsukuba, Ibaraki 305-8571, Japan.
- ^dDepartment of Materials Science and Engineering, Graduate School of Engineering and Resource Science, Akita University, 1-1 Tegata Gakuen-machi, Akita, 010-8502, Japan.
- ^eNational Institute for Materials Science (NIMS), Tsukuba, Ibaraki 305-0044, Japan
- † Electronic Supplementary Information (ESI) available: [Experimental and characterization details]. See DOI: 10.1039/b000000x/
- J. A. Hollingsworth, *Chem. Mater.* 2013, **25**, 1318.
 - M. D. Regulacio, M.-Y. Han, *Acc. Chem. Res.* 2010, **43**, 621.
 - S. S. Lo, T. Mirkovic, C.-H. Chuang, C. Burda, G. D. Scholes, *Adv. Mater.* 2011, **23**, 180.
 - P. Li, Z. Wei, T. Wu, Q. Peng, Y. Li, *J. Am. Chem. Soc.* 2011, **133**, 5660.
 - D. C. Lee, I. Robel, J. M. Pietryga, V. I. Klimov, *J. Am. Chem. Soc.* 2010, **132**, 9960.
 - T. Teranishi, M. Sakamoto, *J. Phys. Chem. Lett.* 2013, 2867.
 - S. C. Glotzer, M. J. Solomon, *Nat Mater* 2007, **6**, 557.
 - F. Li, D. P. Josephson, A. Stein, *Angew. Chem. Int. Ed.* 2011, **50**, 360.
 - M. D. Refulacio, C. Ye, S. H. Lim, M. Bosman, L. Polavarapu, W. L. Koh, J. Zhang, Q.-H. Xu, M.-Y. Han, *J. Am. Chem. Soc.* 2011, **133**, 2052.
 - M. Saruyama, M. Kanehara, T. Teranishi, *J. Am. Chem. Soc.* 2010, **132**, 3280.
 - D. Wang, Y. Li, *Adv. Mater.* 2011, **23**, 1044.
 - M. Saruyama, -G. Y. So, K. Kimoto, S. Taguchi, Y. Kanemitsu, T. Teranishi, *J. Am. Chem. Soc.* 2011, **133**, 17598.
 - D. H. Son, S. M. Hughes, Y. Yin, A. P. Alivisatos, *Science* 2004, **306**, 1009.
 - K. Miszta, D. Dorfs, A. Genovese, M. R. Kim, L. Manna, *ACS Nano* 2011, **5**, 7176.
 - B. K. Hughes, J. M. Luther, M. C. Beard, *ACS Nano* 2012, **6**, 4573.
 - H. Zhong, M. Nagy, M. Jones, G. D. Scholes, *J. Phys. Chem. C* 2009, **113**, 10465.
 - Y. Yan, G. Chen, P. G. Van Patten, *J. Phys. Chem. C* 2011, **115**, 22717.
 - A. H. Nethercot Jr. *Phys. Rev. Lett.* 1974, **33**, 1088.
 - E. Shafran, N. J. Borys, J. Huang, D. V. Talapin, J. M. Lupton, *J. Phys. Chem. Lett.* 2013, **4**, 691.
 - A. M. Smith, S. Nie, *Acc. Chem. Res.* 2009, **43**, 190.
 - K. Tvrdy, P. A. Frantsuzov, P. V. Kamat, *Proc. Natl. Acad. Sci. USA.* 2011, **108**, 29.